ACS APPLIED MATERIALS & INTERFACES

www.acsami.org

Research Article

Infrared Thin Film Detectors Based on Thermoresponsive Microgels with Linear Shrinkage Behavior and Gold Nanorods

Pan Gu, Jiping Wang, Peter Müller-Buschbaum, Dongming Qi,* and Qi Zhong*

Cite This: *ACS Appl. Mater. Interfaces* 2020, 12, 34180–34189

Read Online

ACCESS | Metrics & More | Article Recommendations | Supporting Information

ABSTRACT: To overcome the drawbacks of existing infrared detectors, infrared thin film detectors based on microgels and gold nanorods (Au NRs) are investigated. The microgels with a linear shrinkage of the hydrodynamic diameter between 10 and 55 °C are copolymerized by monomers di(ethylene glycol) methyl ether methacrylate, oligo(ethylene glycol) methyl ether methacrylate, and acrylic acid with a molar ratio of 1:1:1. Homogenous thin films are obtained by spin coating from an aqueous solution on silicon substrates. Upon heating in a water vapor atmosphere, the film thickness of the hybrid films linearly decreases. Heat generation from a plasmon resonance enhanced absorption of the infrared radiation by the Au NRs triggers a linear shrinkage in the hybrid microgel-Au NR films as well. A linear correlation between the film thickness and the applied infrared power density is observed. The sensitivity is enhanced by a slight increase in the amount of Au NRs in the films. Infrared detectors are constructed from the hybrid microgel-Au NR films by adding two electrodes via deposition of two silver layers at the film ends. By monitoring the ohmic resistance, the intensity of the incident infrared light can be obtained. The detectors not only possess a good reversibility and fast response rate but also show a high stability after the resistance measurements. Compared with the traditional infrared detectors, the infrared thin film detectors based on microgels are sensitivity adjustable. Thus, they can be promising candidates for replacing expensive inorganic infrared detectors in areas of daily life applications.

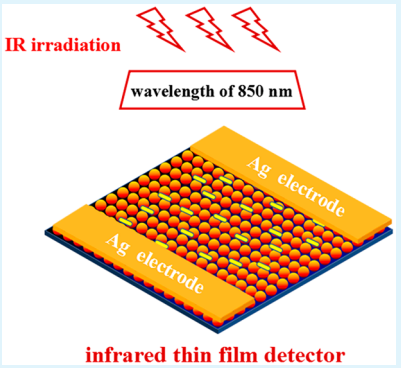

KEYWORDS: *infrared detector, linear shrinkage, microgels, thermoresponsive, gold nanorods, thin films*

INTRODUCTION

In the past few decades, infrared detection technology has been rapidly developed. Traditional thermal detectors can image spectrally uniform objects. Thus, spectral selectivity would be crucial in many applications,[1] such as target recognition and chemical detection. Infrared detector technology was initially developed for military demands, such as target acquisition,[2] surveillance,[3] night vision,[4] and missile warning systems.[5] Recently, the application of infrared technology has been extended to civilian fields, including environmental sensing,[6] health monitoring,[7−9] medical diagnostics,[10] infrared spectroscopy,[11,12] and biomedical imaging.[13] There are mainly two approaches to implement infrared detectors: photon detection and thermal sensing.[2] Infrared detectors based on photodetection utilize the interaction between photons and electrons in a semiconductor material to generate an electrical output signal when being exposed to infrared irradiation.[14,15] The advantages include high resolution, stable performance, and fast response rate. However, in order to achieve such a high performance, they typically require a cryogenic cooling system to prevent thermally produced charge carriers,[16] which causes the detectors to be power inefficient, bulky, and expensive. On the other hand, infrared detectors based on thermal detection depend on the physical changes of the material when being exposed to infrared irradiation. Because of the capability of operation at room temperature, they are generally more power efficient, more compact, and less expensive than those based on photon detection. However, they suffer from a relatively slower response rate and worse resolution. For instance, thermal detectors, such as pyroelectric detectors,[17] bolometers,[18] thermopiles,[19] and the latest resonant detectors (optical[20] and electromechanical[21]), have been demonstrated recently. For example, Hui et al. prepared an ultrathin piezoelectric plasma surface, which was further used to produce a nanomechanical resonator with customized optical and electromechanical properties.[2] Therefore, an efficient on-chip transduction of nanoelectromechanical systems with a plasma resonant structure was achieved. The cumbersome and complex off-chip optical readouts applied in the previous devices was no longer required. These properties can be used further to prepare infrared detectors with a fast response rate, high resolution, and without the need for a cooling system. It is well-known that materials with nanomechanical structure have

Received: May 1, 2020
Accepted: July 7, 2020
Published: July 7, 2020

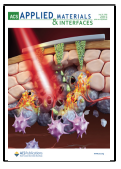

https://dx.doi.org/10.1021/acsami.0c08049
ACS Appl. Mater. Interfaces 2020, 12, 34180–34189

a strong and nonpolarized absorption coefficient in ultrathin thickness, which can effectively converse the infrared radiation into vibrations. Although such approach solves all the drawbacks of resonant infrared detectors mentioned above, the preparation process of related devices is still complicated and time-consuming.

For this reason, simple structure and easy preparation are highly desired for new types of infrared detectors with target applications in daily life products. For example, Xia et al. developed a graphene plasma detector with a capability to detect infrared photons with fast response and high resolution at room temperature.[22] In addition, this detector also had a surprisingly simple design. However, such detectors based on the natural doping of graphene are relatively difficult to be used because they rely on the synthesis process and the sample environment. For this reason, the spectral range might not be uniform among the obtained detectors, which may induce an instability especially for a long operation period. Thus, the future challenge for manufacturing infrared detectors is improving their stability and uniformity. Besides that, instead of the stiffness of the inorganic materials, the device flexibility would also be of great interest for the next generation of infrared detectors. Such detectors could be easily installed in novel areas of application such as textiles and other soft media to prepare smart textiles. For instance, the inorganic material HgCdTe was broadly used as the most suitable semiconductor material for infrared detectors due to the broad range of operation temperature and high resolution in detection performance.[23−25] However, because of its inherent rigidity and fragility, such type of detectors are easy to wear out. As a consequence, novel soft materials are required to enable new infrared detectors with high flexibility in the future.

Recently, inorganic precious metal nanomaterials have been intensively investigated as infrared absorbing materials.[26] Unlike gold in the bulk, gold nanoparticles (Au NPs) can absorb light with certain wavelengths due to the local surface plasmon resonance.[27−29] The heat produced by the plasmon resonance can increase the local temperature of the systems.[30] On the basis of this special property, a variety of applications have been developed using Au NPs with various sizes and shapes, such as optical sensing and biosensing,[31] gene targeting,[32] drug delivery,[33] cell labeling,[34,35] and optical imaging systems.[36] For instance, Richtering et al. synthesized DNA-functionalized gold nanoparticles (DNA-Au NPs), which can assemble into core−shell structures. Thus, they have potential applications in the field of drug release and gene regulation.[37] Besides such assembled structures, Au NPs were also directly introduced into microgels to realize new functions. For example, Hellweg et al. prepared multi-responsive hybrid colloids based on gold nanorods and poly(NIPAM-*co*-allylacetic acid) microgels, which presented temperature- and pH-tunable plasmon resonances. Therefore, they can be used to design novel sensors.[38] In addition, von Klitzing et al. synthesized microgel-based hybrid particles containing Au NPs. The irradiation of Au NPs by a wavelength of 532 nm induced the heat emission and collapse of the microgels.[39] This observation indicates that the phase transition realized by the light−heat transfer from Au NPs is feasible.

In our previous investigation, a linear shrinkage behavior upon heating was observed in thermoresponsive microgels.[40] Because of the presence of two thermoresponsive monomers, di(ethylene glycol) methyl ether methacrylate (MEO_2MA) and oligo(ethylene glycol) methyl ether methacrylate ($OEGMA_{300}$), with different transition temperatures ($TT_{PMEO2MA}$ = 25 °C and $TT_{POEGMA300}$ = 60 °C), the subsequent collapse of $PMEO_2MA$ and $POEGMA_{300}$ upon heating caused these microgels to show a linear shrinkage between both transition temperatures ($TT_{PMEO2MA}$ and $TT_{POEGMA300}$). Unlike the linear transition behavior realized by the core−shell structure in the thermoresponsive microgels reported earlier,[41] the microgels used in our present investigation are synthesized by simply mixing two acrylate-based thermoresponsive monomers, inspired by the work from Wu et al.[42] Therefore, the synthesis takes only one step, which is much faster and more efficient as compared with other approaches. Moreover, as the TT of the acrylate-based thermoresponsive polymers is correlated to the number of ethoxy groups in the side chain,[43] the temperature region showing the linear shrinkage can be easily adjusted by selecting different types of acrylate-based thermoresponsive monomers in the microgels.

In the present study, we make use of this unique behavior and expand the pure microgels into hybrid materials based on Au NPs and thermoresponsive microgels. If both are mixed and spin-coated into films, the heat produced by the Au NPs after the infrared irradiation can trigger the phase transition of the microgel film. In addition, an increase in the infrared irradiation will result in an increase of absorbed radiation by the Au NPs and cause thereby a higher temperature of the film, which in turn causes a linear shrinkage of the microgel film. As the volume of the repelled water shows a linear relationship to the film thickness and the resistance of water is much larger than that of polymer, simply monitoring the ohmic resistance of the microgel film, the intensity of the incident infrared radiation can be obtained. Compared with the former studies about the microgels and Au NPs, the linear shrinkage behavior of the thermoresponsive microgels is the key point to realize the infrared detection in our present investigation.

On the basis of this approach, we present a novel type of polymer-based infrared detector. The microgels with a linear shrinkage behavior are prepared by cross-linking of MEO_2MA, $OEGMA_{300}$, and acrylic acid (AA). The obtained microgels are mixed with gold nanorods (Au NRs) in aqueous solution. By simply spin-coating the mixed solution onto the precleaned Si substrates, thin film infrared detectors are obtained. The intensity of the incident infrared irradiation is accessed by monitoring the resistance of the infrared detector. We study the sensitivity of the infrared detectors and their cyclability. Compared with the traditional infrared detectors, the infrared thin film detectors based on microgels and Au NRs are also sensitivity adjustable. Moreover, in the future, they can be also installed onto a soft medium, such as the textiles. Thus, they can be promising candidates to replace the expensive inorganic infrared detectors and bring them into novel areas of application.

EXPERIMENTAL SECTION

Materials. The monomers di(ethylene glycol) methyl ether methacrylate (MEO_2MA, purity 97.0%) and the initiator ammonium persulfate (APS, purity 99.9%) were obtained from Aladdin. The monomer oligo(ethylene glycol) methyl ether methacrylate ($OEGMA_{300}$, average M_n = 300) and acrylic acid (AA, purity 99.0%) as well as the cross-linker for microgels *N*,*N*-methylene bis-acrylamide (MBA, purity 99.0%) were bought from Sigma-Aldrich. Before the polymerization of microgels, MBA was purified by recrystallization from acetone and dried in vacuum. The other

https://dx.doi.org/10.1021/acsami.0c08049
ACS Appl. Mater. Interfaces 2020, 12, 34180−34189

monomers and agents mentioned above were used as received. Silicon wafer (Si 100, p-type) was bought from Regency Photoelectric technology Co. Ltd., Zhejiang, China. The water-soluble gold nanorods (Au NRs) were purchased from Zhongke Leiming (Beijing) Technology Co., Ltd., with a diameter of 13 nm and a length of 56 nm. The Milli-Q water was from Millipore (Merck KGaA, Germany) with a resistance of 18.2 MΩ cm.

Synthesis of P(MEO_2MA-*co*-$OEGMA_{300}$-*co*-AA) Microgels. The synthesis and purification of P(MEO_2MA-*co*-$OEGMA_{300}$-*co*-AA) microgels is similar to those presented in our previous publication.[40] The details for the synthesis and purification can be found in Supporting Information.

Substrate Cleaning. The silicon wafers with a size of 1.5 × 2.0 cm^2 were first placed in the dichloromethane solution thermostated at 65 °C for 30 min to remove the possible organic traces on surface. After that, they were moved into a basic solution containing H_2O (350 mL), $NH_3{\cdot}H_2O$ (30 mL), and H_2O_2 (30 mL) at 76 °C for 120 min. Then, the Si wafers were placed in the Millipore water. Before spin-coating, they were dried by nitrogen flow to remove the residual water on the surface. On the basis of this protocol, a hydrophilic SiO_2 layer with a thickness of 10 Å was formed on the surface.[44,45]

Preparation of Microgel Films and Infrared Thin Film Detectors. To prepare the microgel films, the purified microgels were first dissolved in water. Homogenous microgel films were obtained by spin-coating the aqueous solution onto the precleaned Si wafers with the spin coater (KW-4A, Institute of microelectronics of Chinese Academy of Sciences, 2000 rpm, 30 s). The thickness of the microgel films (30 to 50 nm) was facilely adjusted by varying the concentration of the aqueous solutions from 50 to 100 mg mL^{-1}.

To prepare the infrared thin film detectors, the ultrasound dispersed Au NRs solution was first added into the microgels' solution. After addition, the mixed solution was again dispersed by ultrasound to obtain a homogeneous mixture. The Au NR concentration in the mixed solution was varied from 0.05 wt % to 0.2 wt %. Then the solution was spin-coated onto the precleaned Si substrates. Homogenous and flat microgel films containing Au NRs were obtained. To explore the potential application as the infrared thin film detectors, homogeneous silver layers were deposited on two ends of the films. During the deposition, the microgel films containing Au NRs was placed upside down in the thermal evaporator (ZHDS-400, Beijing Technol. Co., Ltd. China) under a vacuum of 10^{-4} Pa. By adjusting the applied current and time, the deposited silver layer thickness can be precisely controlled. With a deposition rate and time of 1 Å s^{-1} and 1000 s, a silver layer with a thickness of 1000 Å was realized. The distance between these two electrodes was 15 mm. The detector size was 15 × 20 mm^2, which is a typical size for a laboratory detecting device.

Dynamic Light Scattering (DLS) Measurements. The hydrodynamic diameters (D_H) of P(MEO_2MA-*co*-$OEGMA_{300}$-*co*-AA) microgels were measured by DLS measurements (Malvern, Zetasizer Nano S, U.K.). Before the measurements, the aqueous solution was diluted to 50 mg mL^{-1} and dispersed by ultrasound at 40 Hz for 30 min. After that, it was measured at 10 °C to obtain the size of the as-prepared microgels. Then the solution was heated from 10 to 60 °C with a step of 5 °C. The measurements were performed 2 min after each increase of temperature to ensure the transition of microgels to reach an equilibrium state.

Surface Morphology Measurements for Microgel Films and Infrared Thin Film Detectors. On large scale, the film surfaces were probed with optical microscopy (4XB, Shanghai Optical Instrument Factory, China).

The morphologies of the microgel films and infrared thin film detectors were probed by SEM (VLTRA55, Carl Zeiss SMT Pte Ltd., Germany) with a magnification of 10 000 and 5000, respectively. The working distance and the voltage applied were 8.7 mm and 3 kV for the microgel films as well as 5.5 mm and 3 kV for the infrared thin film detectors.

The morphologies of the microgel films containing Au NRs were also probed by TEM (JEM-2100, Japanese electronics, Japan). The working voltage applied in the measurement was 200 kV. To allow for TEM measurements, the microgel films with Au NRs were prepared on Cu meshes.

Hydration and Collapse of Microgel Films and Infrared Thin Film Detectors. The hydration and collapse behaviors of the microgel film were monitored by White light interferometry (WLI, Filmetrics F20, Filmetrics Inc., San Diego, CA). The microgel film was first fabricated in the customized aluminum chamber (60 × 60 × 17 mm^3, L × W × H) before the measurements. The chamber was thermostated at 20 °C by using a thermal bath (F12 MC, Julabo Labortechnik GmbH, Seelbach, Germany). After that, 6 mL of deionized water was injected into the reservoir to install a moderate vapor atmosphere in the chamber (RH = 95%). Therefore, the hydration set in. The evolution of the film thickness was monitored by WLI. When the hydration reached an equilibrium state, the chamber was heated by the thermal bath. The temperature was increased from 20 to 60 °C with a step of 5 °C. The microgel film was measured 30 min after each increase of temperature to ensure that the film achieved an equilibrium state. The collapse of the film was also monitored by WLI.

To investigate the capability of infrared detection, a thin microgel film was also hydrated in the same scenario. Then, it was irradiated by the infrared light with different power densities. The wavelength of the infrared radiation applied in our investigation was 850 nm. The distance between the infrared light and thin microgel film was 15 mm. The irradiation time was set to 5 min. After each irradiation, the film thickness was measured by WLI immediately. Then, the thin microgel film was equilibrated for 55 min to ensure the fully recovery. To address the influence of Au NRs to the infrared irradiation, the infrared thin film detectors prepared from mixed solutions containing different amounts of Au NRs (0.05 and 0.2 wt %) were measured as well with the same protocol.

UV−vis Spectra for Au NRs Aqueous Solution and Thin Films. The UV−vis spectrum of the Au NRs aqueous solution was monitored with a UV−vis spectrophotometer (UV/vis Lambda 35, PerkinElmer Inc., U.S.A.) in a wavelength range between 300 and 1000 nm.

The UV−vis diffuse reflectance spectra of the pure microgel film, pure Au NR film, and the microgel film containing Au NRs on glass were monitored with an UV−vis spectrophotometer (UV-2600, Shimadzu, Japan) in a wavelength range between 300 and 900 nm.

Resistance Measurements of Infrared Thin Film Detectors. The infrared thin film detector was first mounted in a customized container thermostated at 20 °C. Ten milliliters of deionized water was injected into the reservoir to install a moderate vapor atmosphere (RH = 95%). The resistance of the thin film detector was measured by an ohmmeter. After the resistance reached equilibrium, the film was irradiated by the infrared light with different power densities. The wavelength of the infrared radiation applied was 850 nm. The distance between the infrared light and thin film detector was 30 cm. The corresponding change of resistance was recorded. The setup for the resistance measurement was presented in Figure S1.

To further study the influence of the infrared radiation to the detection capability, the infrared detection measurements of thin microgel films containing 0.2 wt % Au NRs were performed by infrared radiation with a different wavelength (940 nm) as well. The measurement protocol was the same as that mentioned above.

To investigate the difference of the infrared detection capability between Au NRs and Au nanospheres (NSs, diameter of 10 nm), control experiments with microgel films containing 0.2 wt % Au NSs were performed by the infrared radiation with a wavelength of 850 nm. The measurement protocol was the same as that mentioned above.

To investigate the stability of the infrared thin film detectors, the detector was first hydrated in water vapor for different periods (0, 2, and 5 h). Then the resistance was measured with the same protocol described above.

https://dx.doi.org/10.1021/acsami.0c08049
ACS Appl. Mater. Interfaces 2020, 12, 34180−34189

RESULTS AND DISCUSSION

Morphological Characterization. On a large scale, all films are homogeneous (Figure S2). Figure 1 presents

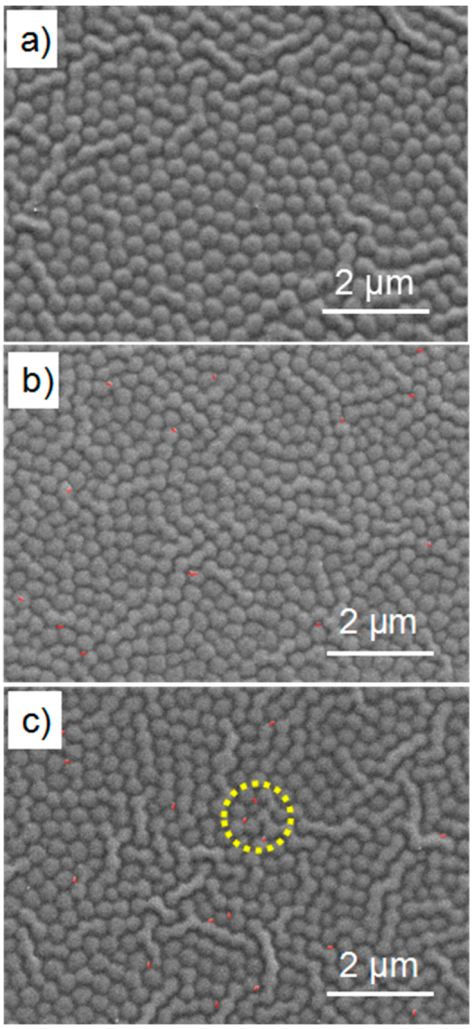

Figure 1. SEM images of the (a) spin-coated P(MEO_2MA-*co*-$OEGMA_{300}$-*co*-AA) microgel film and infrared thin film detectors prepared from solutions containing different amounts of Au NRs concentrations: (b) 0.05 wt %; and (c) 0.2 wt %. Au NRs in the infrared thin film detectors are colored in red, and in one spot, they are highlighted by the dashed yellow circle.

representative SEM images of the microgel films and infrared thin film detectors containing different amounts of Au NRs. Because of the spin-coating process, the microgels are homogeneously distributed on the Si substrate (Figure 1a). No other material is visible on the film. In addition, the size of the microgel particles is rather uniform (diameter 450 ± 10 nm). After adding the Au NRs, tiny dots can be observed in the gaps between the microgels (colored by red in Figure 1b,c). These dots are Au NRs. It should be noted that fewer dots are observed in Figure 1b as compared with Figure 1c because of the lower concentration of Au NRs applied (0.05 wt %) in the film preparation. In earlier studies with spherical Au NPs with microgels composed of chemically cross-linked PNIPAM, an adsorption of the Au NPs onto the microgels[46] or even incorporation of the Au NPs into the microgels was reported.[39] The possible reason for the absence of adsorption and incorporation is the different shape and size of the Au NPs used in the previous investigations and our present study. In previous investigations, the Au NPs possess a sphere structure with a diameter of 10−15 nm.[39,46] However, to realize the infrared detection in our study, Au NRs with a diameter of 13 nm and a length of 56 nm are applied. Therefore, the length/diameter ratio of the Au NRs is larger. Combining the fact that the mixed solution of P(MEO_2MA-*co*-$OEGMA_{300}$-*co*-AA) microgels and Au NRs are spin-coated immediately after the ultrasound dispersion, the adsorption and incorporation are more difficult to be realized in our present study. In order to confirm the existence of Au NRs and study the aggregation of Au NRs in the microgel films, TEM images of the microgel films containing Au NRs on Cu mesh are performed. Figure S3a shows the thermoresponsive P(MEO_2MA-*co*-$OEGMA_{300}$-*co*-AA) microgels together with Au NRs coexisting in the film. At higher magnification (Figure S3b), the formed Au NR aggregates are seen.

Hydration and Collapse. To ensure that the obtained microgels possesses a linear shrinkage behavior upon heating, the hydrodynamic diameter (D_H) of the P(MEO_2MA-*co*-$OEGMA_{300}$-*co*-AA) microgels upon heating is measured by DLS. As presented in Figure S4, D_H shows a linear shrinkage when the temperature is between 10 and 55 °C, which is similar as our previously investigated P(MEO_2MA-*co*-$OEGMA_{300}$-*co*-EGMA) microgels.[40]

After confirming the linear shrinkage of P(MEO_2MA-*co*-$OEGMA_{300}$-*co*-AA) microgels, white light interferometry (WLI) is used to probe the hydration and collapse of the microgel film and infrared thin film detector by monitoring the evolution of the film thickness at a constant temperature and upon heating, respectively. The red dots in Figure 2a present

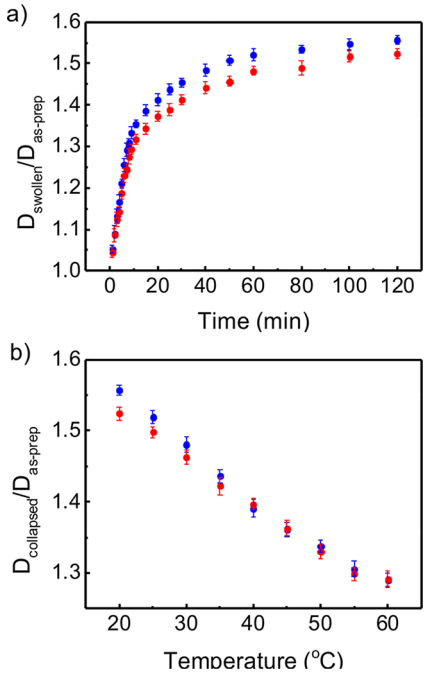

Figure 2. (a) Temporal evolution of the normalized film thickness $D_{swollen}/D_{as\text{-}prep}$ during the hydration in a water vapor atmosphere at 20 °C and (b) normalized film thickness $D_{collapsed}/D_{as\text{-}prep}$ upon heating from 20 to 60 °C of the pure microgel film (red dots) and infrared thin film detector prepared from solution containing 0.1 wt % Au NRs (blue dots).

https://dx.doi.org/10.1021/acsami.0c08049
ACS Appl. Mater. Interfaces 2020, 12, 34180−34189

the temporal evolution of the normalized film thickness $D_{swollen}/D_{as\text{-}prep}$ (pure microgel film) during the hydration in a water vapor atmosphere (RH = 95%) at 20 °C. The initial film thickness of the pure microgel film is 50 ± 1 nm, demonstrating that the microgel particles are flattened in the thin film geometry.[47] Because of the absorption of water vapor, a fast increase of film thickness is observed in the first 10 min. $D_{swollen}/D_{as\text{-}prep}$ can reach 1.31 ± 0.02. After that, a gradual increase of the film thickness is observed. By further prolonging the hydration time to 120 min, $D_{swollen}/D_{as\text{-}prep}$ can reach 1.52 ± 0.02. Still, the microgel particles have not reached a circular shape as known from other microgel particles as well.[48] A similar two-stage hydration behavior was observed in our former investigations about acrylate-based thermoresponsive polymer films.[49,50] To ensure that the added Au NRs will not influence the hydration, the temporal hydration of the infrared thin film detector (prepared from solution containing 0.1 wt % Au NRs) is also probed by WLI (blue dots in Figure 2a). The initial film thickness of the infrared thin film detector is 48 ± 1 nm. Compared to the pure microgel film, the additional Au NRs do not affect the hydration process. The two-stage hydration (first fast and then gradual increase) is also observed. Besides that, the final value of $D_{swollen}/D_{as\text{-}prep}$ (1.56 ± 0.02) is almost the same as that without Au NRs. As the added Au NRs are located outside the microgels, no effect of the Au NRs to the hydration is reasonable. This behavior is also different from the earlier work about thermoresponsive microgels with adsorbed Au NPs, in which swelling capability was significantly reduced after the adsorption of Au NPs.[46] The observed improvement is attributed to the reduced amount of Au NRs located in the gaps in our present study.

After the hydration reaches an equilibrium state, the temperature of the chamber is stepwise increased from 20 to 60 °C with steps of 5 °C. Similar to the P(MEO_2MA-*co*-$OEGMA_{300}$-*co*-AA) microgels in aqueous solution, the pure microgel film (red dots in Figure 2b) also presents a linear shrinkage behavior upon heating. It can be attributed to the synergic effect of the collapsed $PMEO_2MA$ component to the still swollen $POEGMA_{300}$ component when the temperature is between $TT_{PMEO2MA}$ (25 °C) and $TT_{POEGMA300}$ (60 °C). When the temperature reaches 60 °C, $POEGMA_{300}$ also collapses. Thus, the linear shrinkage behavior ends. Besides the pure microgel film, the infrared thin film detector containing 0.1 wt % Au NRs (blue dots in Figure 2b) shows almost the same shrinkage behavior upon heating. Thus, it can be concluded that the additional Au NRs do not influence the transition behavior of the thermoresponsive polymer in the microgel films. This behavior also deviates from the previously reported microgels with adsorbed Au NPs, which showed a lower extent of collapse after the adsorption.[46]

Response of Film Thickness to Infrared Radiation. After confirming the existence of a linear shrinkage behavior in the microgel films whether they contained Au NRs or not, the response of the film thickness to the infrared irradiation with different intensity powers is studied. To confirm that the Au NRs applied in our investigation are sensitive to the infrared radiation, the UV−vis spectrum of the Au NRs in aqueous solution was measured (Figure S5). The Au NRs present a prominent surface plasmon resonance band at around 750 nm. The optical properties of the pure microgel film, pure Au NR film, and microgel film containing Au NRs are investigated with measuring UV−vis diffuse reflectance spectra. As shown in Figure S6, the reflectivity of the pure microgel film is around 90% in the wavelength range of 400−900 nm, which indicates the low absorption in this range. The reflectivity of the microgel film containing Au NRs is reduced to around 80%. In particular, it shows a marked decrease of reflectivity between 700 and 900 nm due to the surface plasmon resonance of the Au NRs. By aggregation of the Au NRs, the resonance broadens as compared with Au NRs in aqueous solution (Figure S5), which is beneficial for having sensitivity over a broad infrared wavelength range. The reflectivity of the pure Au NR film is only around 40%, again with a broad decrease between 600 and 900 nm due to aggregation of the Au NRs. Thereby, the sensitivity to infrared radiation of the microgel film containing Au NRs is confirmed. Moreover, the wavelength of the infrared radiation applied in our investigation (850 nm) matches with the broadened surface plasmon resonance band of the Au NRs aggregates in the microgel films.

As presented in Figure S7, the same two-step hydration process is observed in these three microgel films. Interestingly, the final value of $D_{swollen}/D_{as\text{-}prep}$ are 1.51 ± 0.02 (prepared from a solution containing 0 wt % Au NRs), 1.59 ± 0.01 (prepared from a solution containing 0.05 wt % Au NRs), and 1.67 ± 0.02 (prepared from a solution containing 0.2 wt % Au NRs). It is obvious that the maximum hydration extent increases with the amount of Au NRs. This behavior deviates from our previous observation that the amount of Au NRs does not influence the hydration capability of the microgel films. The possible reason for the increased extent of hydration is the difference of the film thickness. The microgel film thickness decreases from 50 ± 1 nm (0 wt % Au NRs) to 40 ± 1 nm (0.05 wt % Au NRs) and 30 ± 1 nm (0.2 wt % Au NRs). According to our previous investigation, the extent of hydration is strongly correlated to the film thickness because of the hydrophilic effect of Si substrate.[51] This effect is significantly reduced when the film thickens. For this reason, a greater extent of hydration is observed in the infrared thin film detectors with a larger film thickness.

After the hydration reaches an equilibrium state, the swollen films are irradiated by infrared light with different power densities (PD). The starting point of $(D_{swollen} - D_{collapsed})/D_{as\text{-}prep}$ in the pure microgel film is only 0.06 ± 0.01 when the infrared power density is 0.004 W cm^{-2} (blue dots in Figure 3). Because this value is used to evaluate the change of film thickness after the infrared irradiation, the small value indicates

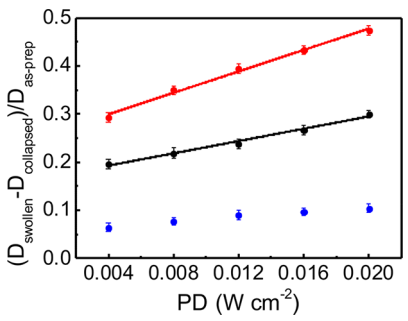

Figure 3. Shrinkage of the pure microgel film (blue dots) and infrared thin film detectors prepared from solutions containing different amounts of Au NRs (black dots, 0.05 wt % and red dots, 0.2 wt %) as a function of infrared power density (PD) under 850 nm infrared irradiation. The solid lines are guides for the eyes.

https://dx.doi.org/10.1021/acsami.0c08049
ACS Appl. Mater. Interfaces 2020, 12, 34180−34189

that the pure microgel film is not sensitive to the infrared irradiation. By further increasing the incident infrared power density, $(D_{swollen} - D_{collapsed})/D_{as\text{-}prep}$ shows only a very minor increase. It might be caused by the tiny increase of the microgels' temperature after the increase of the infrared irradiation, although the container is thermostated at 20 °C. However, since the increase of $(D_{swollen} - D_{collapsed})/D_{as\text{-}prep}$ is only very minor, the pure microgel film is not very responsive to infrared irradiation. On the contrary, two prominent differences are observed in the infrared thin film detector prepared from solution containing 0.05 wt % Au NRs. First, the starting point of $(D_{swollen} - D_{collapsed})/D_{as\text{-}prep}$ increases to 0.2 ± 0.01 when the infrared power density is 0.004 W cm^{-2}. The increase of $(D_{swollen} - D_{collapsed})/D_{as\text{-}prep}$ illustrates that the embedded Au NRs induce the microgel film to be sensitive to the infrared irradiation. Second, a steep slope of the linear shrinkage is observed when the infrared power density is enhanced from 0.004 to 0.02 W cm^{-2}. The final value of $(D_{swollen} - D_{collapsed})/D_{as\text{-}prep}$ is 0.27 ± 0.01 when the infrared power density is 0.02 W cm^{-2}, which is 35% larger than the value at 0.004 W cm^{-2}. Both behaviors indicate that the resonance of Au NRs by the infrared irradiation heats up the microgel film, inducing the linear shrinkage of the film thickness. Further increasing the amount of Au NRs in the solution to 0.2 wt %, the starting point of $(D_{swollen} - D_{collapsed})/D_{as\text{-}prep}$ further increases to 0.29 ± 0.01. Thus, the Au NRs-induced infrared sensitivity in the infrared thin film detectors can be confirmed. In addition, the slope is even steeper, meaning that the sensitivity can be improved by increasing the amount of Au NRs in the microgel films. It should be noted that the amount of Au NRs in the solution is very small (only 0.2 wt %), indicating the high sensitivity of thin film detectors to the infrared irradiation.

Performance of Infrared Thin Film Detector. Although the infrared thin film detectors respond with a linear shrinkage to the power density of the incident infrared irradiation, the film thickness is relatively difficult to measure in our daily life, especially when the film is in the nanometer scale. For this reason, a feasible approach is required to monitor the linear shrinkage instead of measuring the film thickness. In our previous investigation about the thermoresponsive block copolymer films with linear shrinkage behavior, we found that the linear shrinkage of the film can be precisely monitored by the ohmic resistance of the film.[45] Similar as that, in our present investigation, it will be more facile to measure the ohmic resistance of the microgel film than the film thickness by WLI, for example. To enable it, two silver layers are deposited onto the two ends of the infrared thin film detector acting as the electrodes. By simply connecting an ohmmeter to the two electrodes and monitoring the ohmic resistance during the hydration and infrared irradiation, the infrared sensitivity of the thin film detectors can be obtained.

Figure 4a shows the temporal evolution of the normalized resistance $R_{swollen}/R_{as\text{-}prep}$ of the pure microgel film (blue dots) and the infrared thin film detectors prepared from solutions containing different amounts of Au NRs (black dots, 0.05 wt % and red dots, 0.2 wt %) in water vapor atmosphere at 20 °C. Similar as the film thickness, $R_{swollen}/R_{as\text{-}prep}$ is increasing when the hydration process is prolonged. As forehead discussion, the resistance of pure water is much larger than that of the polymer. Hence, the absorption of water induces the resistance of the microgel film to increases with time. Moreover, $R_{swollen}/R_{as\text{-}prep}$ still shows the two-stage increase during the hydration

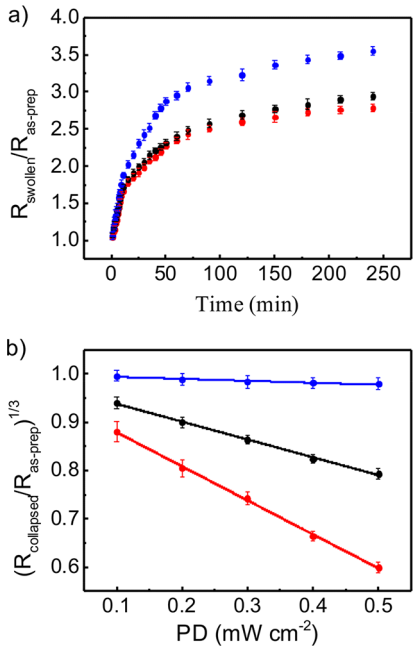

Figure 4. (a) Temporal evolution of normalized resistance $R_{swollen}/R_{as\text{-}prep}$ and (b) $(R_{swollen}/R_{as\text{-}prep})^{1/3}$ as a function of infrared power density in pure microgel film (blue dots) and infrared thin film detectors prepared from solutions containing different amounts of Au NRs (black dots, 0.05 wt % and red dots, 0.2 wt %) in water vapor atmosphere.

irrespective of the presence of Au NRs. Interestingly, the final value of $R_{swollen}/R_{as\text{-}prep}$ in the pure microgel film (3.55 ± 0.06) is larger than the infrared thin film detectors prepared from solutions containing 0.05 wt % Au NRs (2.94 ± 0.05) and 0.2 wt % Au NRs (2.78 ± 0.05). The possible reason is the high conductivity of the Au NRs. After adding them into the microgel films, they can bridge between the microgel particles, which reduces the resistance of the films.

When $R_{swollen}/R_{as\text{-}prep}$ reaches an equilibrium state, the response of the resistance to the power density of the incident infrared irradiation is investigated. Because the linear shrinkage of the microgel particle radius induces the change in volume (resistance) with a power of 3, $(R_{collapsed}/R_{as\text{-}prep})^{1/3}$ is plotted in Figure 4b. Similar to the film thickness, $(R_{collapsed}/R_{as\text{-}prep})^{1/3}$ shows nearly no correlation to the power density in the pure microgel film. Besides that, $(R_{collpased}/R_{as\text{-}prep})^{1/3}$ is around 0.99 ± 0.01 at 0.1 mW cm^{-2}. As the value is very close to 1, it again confirms that the pure microgel film is not sensitive to infrared irradiation. However, when the concentration of Au NRs is 0.05 wt %, $(R_{collapsed}/R_{as\text{-}prep})^{1/3}$ significantly decreases to 0.94 ± 0.01 at 0.1 mW cm^{-2}. Besides that, a linear shrinkage of $(R_{collapsed}R_{as\text{-}prep})^{1/3}$ with increasing infrared power density is observed. It not only means the resonance of Au NRs triggered by the infrared irradiation can heat up the microgel films but also indicates that more heat can be produced by increasing the infrared power density. Further increasing the concentration of Au NRs to 0.2 wt %, $(R_{collapsed}/R_{as\text{-}prep})^{1/3}$ continues to decrease to 0.88 ± 0.02 at 0.1 mW cm^{-2}. In addition, a steeper linear shrinkage of $(R_{collapsed}/R_{as\text{-}prep})^{1/3}$ with PD is observed. Thus, the infrared sensitivity of the thin film detector can be easily adjusted by the amount of Au NRs embedded in the microgel films.

To further study the infrared sensitivity of the thin film detectors, the correlation between $(R_{collapsed}/R_{as\text{-}prep})^{1/3}$ and the

https://dx.doi.org/10.1021/acsami.0c08049
ACS Appl. Mater. Interfaces 2020, 12, 34180−34189

infrared irradiation distance with a fixed infrared irradiation power (5 W) is investigated for the detector prepared from the solution containing 0.2 wt % Au NRs. As shown in Figure 5,

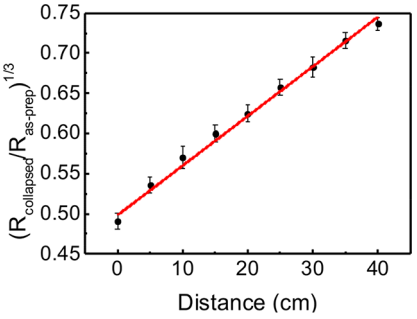

Figure 5. $(R_{collpased}/R_{as\text{-}prep})^{1/3}$ in the infrared thin film detector prepared from the solution containing 0.2 wt % Au NRs as a function of infrared irradiation distance.

$(R_{collapsed}/R_{as\text{-}prep})^{1/3}$ increases linearly with the infrared irradiation distance. When the infrared radiation distance increases, the infrared power density exposed on the thin film detector decreases. Therefore, less heat is generated by the resonance of Au NRs, inducing the smaller change of volume and resistance in the microgels. It shows that the infrared thin film detectors can accurately detect the infrared irradiation at different distances.

To present the influence of the infrared radiation wavelength on the detection capability, measurements are also performed at 940 nm. The infrared thin film detector prepared from the solution containing 0.2 wt % Au NRs shows a linear shrinkage of $(R_{collapsed}/R_{as\text{-}prep})^{1/3}$ with increasing infrared power density as well (Figure S8a). Compared with the behavior at 850 nm, the resistance at every infrared power density is slightly smaller when an off-resonance wavelength is used. As shown in Figure S8b, $(R_{collapsed}/R_{as\text{-}prep})^{1/3}$ still increases linearly with the infrared radiation distance when using 940 nm. It should be noted that all values obtained at 940 nm infrared radiation are slightly larger than at 850 nm, indicating the change of the resistance is smaller off-resonance. Thus, the thin film infrared detector still works well at other wavelengths but shows a reduced sensitivity.

To further investigate the correlation between the shape of the used Au nanoparticles and the infrared detection capability, control experiments with microgel films containing 0.2 wt % Au NSs (maximum local surface plasmon resonance at 520 nm, Figure S9) are performed using infrared radiation with a wavelength of 850 nm. As shown in Figure S10a, $(R_{collapsed}/R_{as\text{-}prep})^{1/3}$ also shows a linear correlation to the power density in the microgel films containing Au NSs, which is similar as in the case of microgel films containing Au NRs. However, the changes in resistance are significantly smaller, which can be attributed to the deviation of the incident wavelength (850 nm) from the wavelength of the maximum local surface plasmon resonance of the Au NSs. Similar to Au NRs, the Au NSs also show aggregation, which not only broaden the local surface plasmon resonance band but also show an additional resonance band around 750 nm.[52] Thus, although there is no absorption observed around 850 nm in the Au NSs aqueous solution, still infrared sensitivity in the microgel films containing Au NSs is obtained. Accordingly, also $(R_{collapsed}/R_{as\text{-}prep})^{1/3}$ shows a linear increase with the infrared irradiation distance in the case of microgel films containing 0.2 wt % Au NSs (Figure S10b). However, all values are larger than the values obtained from the microgel film containing Au NRs using the same infrared radiation because of the smaller influence of the irradiation in case of Au NSs. Therefore, Au NRs enable more sensitive thin film infrared detectors than Au NSs.

Besides sensitivity also the response rate is an important parameter for infrared detectors. Consequently, the response rate of the infrared thin film detectors is studied as well.

Figure 6 shows $R_{collpased}/R_{as\text{-}prep}$ in the infrared thin film detectors with different amounts of Au NRs during the cycles

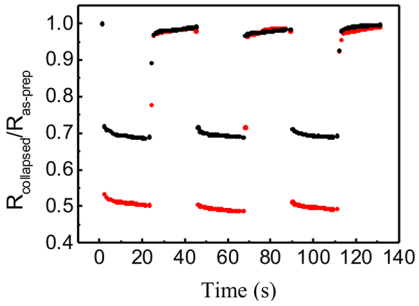

Figure 6. $R_{collpased}/R_{as\text{-}prep}$ in the infrared thin film detectors prepared from solutions containing different amounts of Au NRs (black dots, 0.05 wt % and red dots, 0.2 wt %) during the cycles of infrared irradiation switched on and off in water vapor atmosphere. The power density of the infrared irradiation and the surrounding temperature are fixed as 0.2 mW cm^{-2} and 20 °C, respectively.

of infrared irradiation being switched on and off in water vapor atmosphere. The power density of the infrared irradiation and the surrounding temperature are fixed as 0.2 mW cm^{-2} and 20 °C, respectively. The infrared thin film detector prepared from the solution containing 0.05 wt % Au NRs exhibits a fast response to the infrared irradiation. Only 1 s after the irradiation, $R_{collpased}/R_{as\text{-}prep}$ dramatically drops from 1 to 0.69 ± 0.01. After that, the value almost remains unchanged. When the infrared irradiation is switched off, $R_{collpased}/R_{as\text{-}prep}$ immediately recovers to 0.89 ± 0.03 in 1 s. Only after 2 s, the value is back to 0.97 ± 0.01, which is very close to the initial value. On−off cycles are repeated three times to ensure reproducibility of the fast response. At an increased amount of Au NRs in the solution (0.2 wt %), the fast response to the infrared irradiation is unchanged. The only difference is that the final value of the normalized resistance is further reduced to 0.49 ± 0.01, as expected from the higher detector sensitivity.

After investigating the performance of the infrared thin film detectors, the stability is another important aspect for the real application. Inaccurate detection of infrared irradiation will occur if the infrared thin film detectors are unstable. On the basis of our previous discussion, $(R_{collapsed}/R_{as\text{-}prep})^{1/3}$ presents a linear relation to the infrared power density. Therefore, the stability can be obtained by simply testing the linear relation of the thin film detectors undergoing different hydration times as a function of the infrared power density.

Figure 7 shows the influence of the hydration time on the performance of the infrared thin film detectors. When the hydration time is 0 h, a linear shrinkage of $(R_{collapsed}/R_{as\text{-}prep})^{1/3}$ is observed (black dots), which is also present after hydration in water vapor for 2 h (blue dots) and 5 h (green dots). Irrespective of the hydration time, the linear shrinkage remains almost unchanged. Although there are no covalent bonds

https://dx.doi.org/10.1021/acsami.0c08049
ACS Appl. Mater. Interfaces 2020, 12, 34180−34189

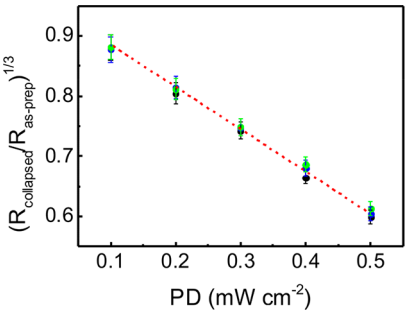

Figure 7. $(R_{collapsed}/R_{as\text{-}prep})^{1/3}$ in infrared thin film detector prepared from the solution containing 0.2 wt % Au NRs as a function of infrared power density after different hydration times (black dots, 0 h; blue dots, 2 h; and green dots, 5 h). The dashed lines are guide lines to show the linear relationship.

between the Si substrate and the microgel, the thin microgel films still present a good stability, which is confirmed by the correlation between the performance of the infrared detector and the hydration time (Figure 7). It is related to the hydrophilicity of the Si substrate by the cleaning protocol applied during the sample preparation, which induces a good affinity between both. Compared with potentially more stable hybrid structures of microgels, such as core−shell or core−satellite structures, the synthesis of P(MEO_2MA-*co*-$OEGMA_{300}$-*co*-AA) microgels takes only one step. Thereby, the synthesis is facile, which renders it interesting for application. Despite the simple synthesis route, the stability of the obtained infrared detector is good. Thus, it can be concluded that our infrared thin film detectors can stably measure the intensity of infrared irradiation in a water vapor environment.

CONCLUSION

Polymer-based infrared thin film detectors with high sensitivity and good stability are achieved by simply spin-coating a solution of Au NRs and thermoresponsive microgels onto Si substrates. Because of the synergistic effect between $PMEO_2MA$ and $POEGMA_{300}$ upon heating, the P(MEO_2MA-*co*-$OEGMA_{300}$-*co*-AA) microgels present a linear shrinkage between 10 and 55 °C. Homogeneous infrared thin film detectors are obtained by adding small amounts of Au NRs to the microgel. The microgel particles have a uniform structure in the film. The Au NRs aggregate and are located in the gaps between the microgel particles. The added Au NRs do not influence the hydration and linear shrinkage of the microgels. By resonance enhanced absorption of infrared radiation by the Au NRs, heat is generated, which triggers the linear shrinkage of the size and the resistance in the microgels. Thus, the intensity of the incident infrared irradiation can be monitored by simply measuring the resistance of the detector. Moreover, the infrared sensitivity of the detector is enhanced by slightly increasing the amount of Au NRs in the microgel films. The infrared thin film detectors show a good sensitivity, a fast response, and an excellent stability. Moreover, in the future, infrared thin film detectors based on P(MEO_2MA-*co*-$OEGMA_{300}$-*co*-AA) microgels can be also easily installed on a soft medium to prepare for example smart textiles for monitoring infrared irradiation.

ASSOCIATED CONTENT

Supporting Information

The Supporting Information is available free of charge at https://pubs.acs.org/doi/10.1021/acsami.0c08049.

Details for the synthesis and purification, setup for the resistance measurement, optical microscopy images of pure microgel film, Au NR film and the microgel film containing Au NRs, TEM images of the microgel film containing Au NRs, hydrodynamic diameter (D_H) of P(MEO_2MA-*co*-$OEGMA_{300}$-*co*-AA) microgels as a function of the temperature, UV-vis spectrum of the Au NRs in aqueous solution, UV-vis diffuse reflectance spectra of the pure microgel film, pure Au NR film and the microgel film containing Au NRs, temporal evolution of the normalized film thickness $D_{swollen}/D_{as\text{-}prep}$ of P(MEO_2MA-*co*-$OEGMA_{300}$-*co*-AA) microgel film during the hydration in a water vapor atmosphere at 20 °C, $(R_{collpased}/R_{as\text{-}prep})^{1/3}$ as a function of infrared power density and infrared irradiation distance in infrared thin film detector containing 0.2 wt% Au NRs irradiated at a wavelength of 940 nm in water vapor atmosphere, UV-vis spectrum of Au NSs in aqueous solution, $(R_{collapsed}/R_{as\text{-}prep})^{1/3}$ as a function of infrared power density and infrared irradiation distance in infrared thin film detector containing 0.2 wt% Au NSs irradiated at a wavelength of 850 nm in water vapor atmosphere. (PDF)

AUTHOR INFORMATION

Corresponding Authors

Qi Zhong − *Key Laboratory of Advanced Textile Materials & Manufacturing Technology, Ministry of Education, Zhejiang Sci-Tech University, 310018 Hangzhou, China; Technische Universität München, Physik-Department, Lehrstuhl für Funktionelle Materialien, 85748 Garching, Germany;* orcid.org/0000-0003-2069-206X; Phone: +86 571 86843436; Email: qi.zhong@zstu.edu.cn; Fax: +86 571 86843436

Dongming Qi − *Key Laboratory of Advanced Textile Materials & Manufacturing Technology, Ministry of Education, Zhejiang Sci-Tech University, 310018 Hangzhou, China*; Phone: +86 571 86843436; Email: dongmingqi@zstu.edu.cn; Fax: +86 571 86843436

Authors

Pan Gu − *Key Laboratory of Advanced Textile Materials & Manufacturing Technology, Ministry of Education, Zhejiang Sci-Tech University, 310018 Hangzhou, China*

Jiping Wang − *Shanghai University of Engineering Science, 201620 Shanghai, China*

Peter Müller-Buschbaum − *Technische Universität München, Physik-Department, Lehrstuhl für Funktionelle Materialien, 85748 Garching, Germany; Heinz Maier-Leibnitz Zentrum (MLZ), Technische Universität München, 85748 Garching, Germany;* orcid.org/0000-0002-9566-6088

Complete contact information is available at: https://pubs.acs.org/10.1021/acsami.0c08049

Author Contributions

The manuscript was written through contributions of all authors. All authors have given approval to the final version of the manuscript.

https://dx.doi.org/10.1021/acsami.0c08049
ACS Appl. Mater. Interfaces 2020, 12, 34180−34189

Funding

This work is supported by the National Natural Science Foundation of China (Grant Nos. 51403186 and 51611130312), the Scientific Research Foundation for the Returned Overseas Chinese Scholars, State Education Ministry and the Fundamental Research Funds of Zhejiang Sci-Tech University (Grant No. 2019Q015). P.M.B. acknowledges support by the Deutsche Forschungsgemeinschaft DFG (Mu1487/23).

Notes

The authors declare no competing financial interest.

REFERENCES

(1) Talghader, J. J.; Gawarikar, A. S.; Shea, R. P. Spectral Selectivity in Infrared Thermal Detection. *Light: Sci. Appl.* **2012**, *1*, e24.
(2) Hui, Y.; Gomez-Diaz, J. S.; Qian, Z.; Alù, A.; Rinaldi, M. Plasmonic Piezoelectric Nanomechanical Resonator for Spectrally Selective Infrared Sensing. *Nat. Commun.* **2016**, *7*, 11249.
(3) Bhan, R. K.; Dhar, V. Recent Infrared Detector Technologies, Applications, Trends and Development of HgCdTe Based Cooled Infrared Focal Plane Arrays and Their Characterization. *Opto-Electron. Rev.* **2019**, *27*, 174−193.
(4) Sargent, E. H. Solar Cells, Photodetectors, and Optical Sources from Infrared Colloidal Quantum Dots. *Adv. Mater.* **2008**, *20*, 3958−3964.
(5) Guo, C.; Sun, Y.; Jia, Q.; Jiang, Z.; Jiang, D.; Wang, G.; Xu, Y.; Wang, T.; Tian, J.; Wu, Z.; Niu, Z. Wide Spectrum Responsivity Detectors from Visible to Mid-infrared Based on Antimonide. *Infrared Phys. Technol.* **2019**, *96*, 1−6.
(6) Tan, C. L.; Mohseni, H. Emerging Technologies for High Performance Infrared Detectors. *Nanophotonics* **2018**, *7*, 169−197.
(7) Park, S.; Fukuda, K.; Wang, M.; Lee, C.; Yokota, T.; Jin, H.; Jinno, H.; Kimura, H.; Zalar, P.; Matsuhisa, N.; Umezu, S.; Bazan, G. C.; Someya, T. Ultraflexible Near-Infrared Organic Photodetectors for Conformal Photoplethysmogram Sensors. *Adv. Mater.* **2018**, *30*, 1802359.
(8) Xu, H.; Liu, J.; Zhang, J.; Zhou, G.; Luo, N.; Zhao, N. Flexible Organic/Inorganic Hybrid Near-Infrared Photoplethysmogram Sensor for Cardiovascular Monitoring. *Adv. Mater.* **2017**, *29*, 1700975.
(9) Yokota, T.; Zalar, P.; Kaltenbrunner, M.; Jinno, H.; Matsuhisa, N.; Kitanosako, H.; Tachibana, Y.; Yukita, W.; Koizumi, M.; Someya, T. Ultraflexible Organic Photonic Skin. *Sci. Adv.* **2016**, *2*, No. e1501856.
(10) Li, Q.; Guo, Y.; Liu, Y. Exploration of Near-Infrared Organic Photodetectors. *Chem. Mater.* **2019**, *31*, 6359−6379.
(11) Wu, Z.; Yao, W.; London, A. E.; Azoulay, J. D.; Ng, T. N. Elucidating the Detectivity Limits in Shortwave Infrared Organic Photodiodes. *Adv. Funct. Mater.* **2018**, *28*, 1800391.
(12) Tang, Z.; Ma, Z.; Sanchez-Diaz, A.; Ullbrich, S.; Liu, Y.; Siegmund, B.; Mischok, A.; Leo, K.; Campoy-Quiles, M.; Li, W.; Vandewal, K. Polymer:Fullerene Bimolecular Crystals for Near-Infrared Spectroscopic Photodetectors. *Adv. Mater.* **2017**, *29*, 1702184.
(13) Wu, Z.; Zhai, Y.; Yao, W.; Eedugurala, N.; Zhang, S.; Huang, L.; Gu, X.; Azoulay, J. D.; Ng, T. N. The Role of Dielectric Screening in Organic Shortwave Infrared Photodiodes for Spectroscopic Image Sensing. *Adv. Funct. Mater.* **2018**, *28*, 1805738.
(14) Reine, M. B. HgCdTe Photodiodes for IR Detector: a review. *Proc. SPIE* **2001**, *4288*, 266−277.
(15) Kozlowski, L. J.; Arias, J. M.; Williams, G. M.; Vural, K.; Cooper, D. E.; Cabelli, S. A.; Bruce, C. F., Jr. Recent Advances in Staring Hybrid Focal Plane Arrays: Comparison of HgCdTe, InGaAs, and GaAs/AlGaAs Detector Technologies. *Proc. SPIE* **1994**, *2274*, 93−116.
(16) Rogalski, A. Infrared Detectors: Status and Trends. *Prog. Quantum Electron.* **2003**, *27*, 59−210.
(17) Kang, D. H.; Kim, K. W.; Lee, S. Y.; Kim, Y. H.; Keun Gil, S. Influencing Factors on the Pyroelectric Properties of Pb (Zr, Ti)O_3 Thin Film for Uncooled Infrared Detector. *Mater. Chem. Phys.* **2005**, *90*, 411−416.
(18) Chen, C.; Yi, X.; Zhao, X.; Xiong, B. Characterization of VO_2 Based Uncooled Microbolometer Linear Array. *Sens. Actuators, A* **2001**, *90*, 212−214.
(19) Schaufelbühl, A.; Schneeberger, N.; Münch, U.; Waelti, M.; Paul, O.; Brand, O.; Baltes, H.; Menolfi, C.; Qiuting Huang; Doering, E.; Loepfe, M.; et al. Uncooled Low-Cost Thermal Imager Based on Micromachined CMOS Integrated Sensor Array. *J. Microelectromech. Syst.* **2001**, *10*, 503−510.
(20) Watts, M. R.; Shaw, M. J.; Nielson, G. N. Optical Resonators: Microphotonic Thermal Imaging. *Nat. Photonics* **2007**, *1*, 632−634.
(21) Hui, Y.; Rinaldi, M. Fast and High Resolution Thermal Detector Based on an Aluminum Nitride Piezoelectric Micro-electromechanical Resonator with an Integrated Suspended Heat Absorbing Element. *Appl. Phys. Lett.* **2013**, *102*, 093501.
(22) Guo, Q.; Yu, R.; Li, C.; Yuan, S.; Deng, B.; García de Abajo, F. J.; Xia, F. Efficient Electrical Detection of Mid-Infrared Graphene Plasmons at Room Temperature. *Nat. Mater.* **2018**, *17*, 986−992.
(23) Rogalski, A. History of Infrared Detectors. *Opto-Electron. Rev.* **2012**, *20*, 3.
(24) Rogalski, A. Hg Cd Te Infrared Detector Material: History, Status and Outlook. *Rep. Prog. Phys.* **2005**, *68*, 2267−2336.
(25) Rogalski, A.; Antoszewski, J.; Faraone, L. Third-generation Infrared Photodetector Arrays. *J. Appl. Phys.* **2009**, *105*, 091101.
(26) Bao, Z.; Liu, X.; Liu, Y.; Liu, H.; Zhao, K. Near-Infrared Light-Responsive Inorganic Nanomaterials for Photothermal Therapy. *Asian J. Pharm. Sci.* **2016**, *11*, 349−364.
(27) Roper, D. K.; Ahn, W.; Hoepfner, M. Microscale Heat Transfer Transduced by Surface Plasmon Resonant Gold Nanoparticles. *J. Phys. Chem. C* **2007**, *111*, 3636−3641.
(28) Hu, M.; Hartland, G. V. Heat Dissipation for Au Particles in Aqueous Solution: Relaxation Time versus Size. *J. Phys. Chem. B* **2002**, *106*, 7029−7033.
(29) Jain, P. K.; Lee, K. S.; El-Sayed, I. H.; El-Sayed, M. A. Calculated Absorption and Scattering Properties of Gold Nanoparticles of Different Size, Shape, and Composition: Applications in Biological Imaging and Biomedicine. *J. Phys. Chem. B* **2006**, *110*, 7238−7248.
(30) Islam, M. R.; Irvine, J.; Serpe, M. J. Photothermally Induced Optical Property Changes of Poly(N-isopropylacrylamide) Microgel-Based Etalons. *ACS Appl. Mater. Interfaces* **2015**, *7*, 24370−24376.
(31) Saha, K.; Agasti, S. S.; Kim, C.; Li, X.; Rotello, V. M. Gold Nanoparticles in Chemical and Biological Sensing. *Chem. Rev.* **2012**, *112*, 2739−2779.
(32) Daniel, M. C.; Astruc, D. Gold Nanoparticles: Assembly, Supramolecular Chemistry, Quantum-Size-Related Properties, and Applications toward Biology, Catalysis, and Nanotechnology. *Chem. Rev.* **2004**, *104*, 293−346.
(33) Thomas, S. W.; Joly, G. D.; Swager, T. M. Chemical Sensors Based on Amplifying Fluorescent Conjugated Polymers. *Chem. Rev.* **2007**, *107*, 1339−1386.
(34) Rosi, N. L.; Mirkin, C. A. Nanostructures in Biodiagnostics. *Chem. Rev.* **2005**, *105*, 1547−1562.
(35) Dubertret, B.; Calame, M.; Libchaber, A. J. Single-Mismatch Detection using Gold-Quenched Fluorescent Oligonucleotides. *Nat. Biotechnol.* **2001**, *19*, 365−370.
(36) Kim, D.; Park, S.; Lee, J. H.; Jeong, Y. Y.; Jon, S. Antibiofouling Polymer-Coated Gold Nanoparticles as a Contrast Agent for in Vivo X-ray Computed Tomography Imaging. *J. Am. Chem. Soc.* **2007**, *129*, 7661−7665.
(37) Buchkremer, A.; Linn, M. J.; Timper, J. U.; Eckert, T.; Mayer, J.; Richtering, W.; Von Plessen, G.; Simon, U. Synthesis and Internal Structure of Finite-Size DNA−Gold Nanoparticle Assemblies. *J. Phys. Chem. C* **2014**, *118*, 7174−7184.
(38) Karg, M.; Lu, Y.; Carbó-Argibay, E.; Pastoriza-Santos, I.; Pérez-Juste, J.; Liz-Marzán, L. M.; Hellweg, T. Multiresponsive Hybrid

Colloids Based on Gold Nanorods and Poly(NIPAM-*co*-allylacetic acid) Microgels: Temperature- and pH-Tunable Plasmon Resonance. *Langmuir* **2009**, *25*, 3163−3167.
(39) Lehmann, M.; Tabaka, W.; Möller, T.; Oppermann, A.; Wöll, D.; Volodkin, D.; Wellert, S.; von Klitzing, R. DLS Setup for in Situ Measurements of Photoinduced Size Changes of Microgel-Based Hybrid Particles. *Langmuir* **2018**, *34*, 3597−3603.
(40) Gu, P.; Fan, N.; Wang, Y.; Wang, J.; Müller-Buschbaum, P.; Zhong, Q. Linear Control of Moisture Permeability and Anti-adhesion of Bacteria in a Broad Temperature Region Realized by Cross-Linking Thermoresponsive Microgels onto Cotton Fabrics. *ACS Appl. Mater. Interfaces* **2019**, *11*, 30269−30277.
(41) Zeiser, M.; Freudensprung, I.; Hellweg, T. Linearly Thermoresponsive core-shell Microgels: Towards a New Class of Nanoactuators. *Polymer* **2012**, *53*, 6096−6101.
(42) Hou, L.; Wu, P. Microgels with Linear Thermosensitivity in a Wide Temperature Range. *Macromolecules* **2016**, *49*, 6095−6100.
(43) Lutz, J. F.; Hoth, A. Preparation of Ideal PEG Analogues with a Tunable Thermosensitivity by Controlled Radical Copolymerization of 2-(2-methoxyethoxy)ethyl Methacrylate and Oligo(ethylene glycol) Methacrylate. *Macromolecules* **2006**, *39*, 893−896.
(44) Kern, W. The Evolution of Silicon Wafer Cleaning Technology. *J. Electrochem. Soc.* **1990**, *137*, 1887−1892.
(45) Zhong, Q.; Chen, C.; Mi, L.; Wang, J.; Yang, J.; Wu, G.-P.; Xu, Z.-K.; Cubitt, R.; Müller-Buschbaum, P. Thermoresponsive Diblock Copolymer Films with a Linear Shrinkage Behavior and its Potential Application in Temperature Sensors. *Langmuir* **2020**, *36*, 742−753.
(46) Gawlitza, K.; Turner, S. T.; Polzer, F.; Wellert, S.; Karg, M.; Mulvaney, P.; von Klitzing, R. Interaction of Gold Nanoparticles with Thermoresponsive Microgels: Influence of the Cross-Linker Density on Optical Properties. *Phys. Chem. Chem. Phys.* **2013**, *15*, 15623−15631.
(47) Wellert, S.; Kesal, D.; Schon, S.; von Klitzing, R.; Gawlitza, K. Ethylene Glycol-Based Microgels at Solid Surfaces: Swelling Behavior and Control of Particle Number Density. *Langmuir* **2015**, *31*, 2202−2210.
(48) Burmistrova, A.; Richter, M.; Eisele, M.; Uzum, C.; von Klitzing, R. The Effect of Co-Monomer Content on the Swelling/Shrinking and Mechanical Behaviour of Individually Adsorbed PNIPAM Microgel Particles. *Polymers* **2011**, *3*, 1575−1590.
(49) Zhong, Q.; Wang, W. N.; Adelsberger, J.; Golosova, A.; Bivigou Koumba, A. M.; Laschewsky, A.; Funari, S. S.; Perlich, J.; Roth, S. V.; Papadakis, C. M.; Müller-Buschbaum, P. Collapse Transition in Thin Films of Poly(methoxydiethylenglycol acrylate). *Colloid Polym. Sci.* **2011**, *289*, 569−581.
(50) Zhong, Q.; Metwalli, E.; Rawolle, M.; Kaune, G.; Bivigou-Koumba, A. M.; Laschewsky, A.; Papadakis, C. M.; Cubitt, R.; Müller-Buschbaum, P. Structure and Thermal Response of Thin Thermoresponsive Polystyrene-*block*-poly(methoxydiethylene glycol acrylate)-*block*-polystyrene Films. *Macromolecules* **2013**, *46*, 4069−4080.
(51) Zhong, Q.; Mi, L.; Metwalli, E.; Bießmann, L.; Philipp, M.; Miasnikova, A.; Laschewsky, A.; Papadakis, C. M.; Cubitt, R.; Schwartzkopf, M.; Roth, S. V.; Wang, J. P.; Müller-Buschbaum, P. Effect of Chain Architecture on the Swelling and Thermal Response of Star-shaped Thermo-responsive (poly(methoxy diethylene glycol acrylate)-*block*-polystyrene)$_3$ block Copolymer Films. *Soft Matter* **2018**, *14*, 6582−6594.
(52) Lin, M.; Guo, C. R.; Li, J.; Zhou, D.; Liu, K.; Zhang, X.; Xu, T. S.; Zhang, H.; Wang, L. P.; Yang, B. Polypyrrole-Coated Chainlike Gold Nanoparticle Architectures with the 808 nm Photothermal Transduction Efficiency up to 70%. *ACS Appl. Mater. Interfaces* **2014**, *6*, 5860−5868.

https://dx.doi.org/10.1021/acsami.0c08049
ACS Appl. Mater. Interfaces 2020, 12, 34180−34189